



# Structural, morphological and optical properties of tungsten trioxide nanoparticle synthesis by pulsed laser ablation in water: effect of laser fluence

Maryam S. Muhsin<sup>1</sup> · Evan T. Salim<sup>1</sup> · Jehan A. Saimon<sup>1</sup>

Received: 12 July 2023 / Accepted: 7 August 2023 / Published online: 29 August 2023  
© The Author(s), under exclusive licence to The Optical Society of India 2023

**Abstract** In this paper, we introduce the pulsed laser ablation in liquid technique for the synthesis of tungsten oxide nanoparticle colloid in water. Tungsten trioxide nanoparticles produced at different laser fluence in DD water at room temperature by pulsed laser ablation of the W target have been studied. The effect of increasing laser fluence on the structural, morphological and optical properties of WO<sub>3</sub> NPs was investigated by using X-ray diffraction (XRD), optical properties, photoluminescence (PL), scanning electron microscope (SEM), energy-dispersive X-ray spectroscopy and transmission electron microscopy (TEM). The XRD data demonstrated that all of the produced WO<sub>3</sub> NPs are polycrystalline and confirm producing WO<sub>3</sub> NPs in all samples at water environments. The absorption spectra of all samples contained the excitonic/plasmonic absorption peak of WO<sub>3</sub> NPs. Direct optical energy gap of WO<sub>3</sub> NPs prepared at different laser fluence was in the range of 3.02–3.1 eV at room temperature. The PL measurement indicates a peak emission centered at 404 nm, and increasing the laser fluence results in a redshift. The PL spectra showed band-to-band transitions and WO<sub>3</sub> oxygen vacancies. The surface morphology of WO<sub>3</sub> NPs investigated by FESEM revealed the formation of spherical NPs morphologies, and the TEM result shows the particle size and concentration of wo3 increased from 6 to 33 nm with increasing laser fluence. The goal of this experiment was to demonstrate how the laser fluence might be used to regulate the centering of WO<sub>3</sub> nanoparticles. In other words, laser fluence are a

helpful tool for managing the centering and particle size of created WO<sub>3</sub> nanoparticles.

**Keywords** WO<sub>3</sub> NPs · Pulsed laser ablation · Nanoparticles · Surface plasmon · Exciton

## Introduction

Yellow powdered tungsten oxide (WO<sub>3</sub>) has a density of 7.16 g/cm<sup>3</sup>, a melting point of 1473 °C and a boiling temperature of 1700 °C. It is insoluble in water and most acids (apart from hydrofluoric acid) but soluble in ammonium hydroxide, where it forms a tungstate [1–5]. Tungsten oxide (WO<sub>3</sub>) has small bandgap between 2.7 and 3.1 eV, and it makes substance that is active in the visible light spectrum. WO<sub>3</sub> is a stable semiconductor material [6]. Since tungsten has a 5d<sup>4</sup> 6s<sup>2</sup> outer electron configuration, it may exist in five distinct valence states in its compound, including +2, +3, +4, +5 and +6, with the possibility of several valence states existing simultaneously. WO<sub>3</sub> is the highest tungsten oxide state. The oxygen ratio in WO<sub>3</sub> is commonly stated in the form of WO<sub>3-x</sub>, such as WO<sub>2.90</sub>, WO<sub>2.83</sub> and WO<sub>2.72</sub>. Due to the lack of oxygen, some W6+ is converted to W5+, resulting in a mixture of W5+ and W6+ [7, 8]. The color of WO<sub>3</sub> varies with the amount of oxygen present. WO<sub>3</sub> looks yellow, WO<sub>2.90</sub> looks purple, WO<sub>2.83</sub> looks dark blue, and WO<sub>2.72</sub> looks blue [9]. Monoclinic II (-WO<sub>3</sub>) is among the frequent WO<sub>3</sub> crystal phases [10, 11], monoclinic I (γ-WO<sub>3</sub>) [12], triclinic (δ-WO<sub>3</sub>) [13, 14], orthorhombic (β-WO<sub>3</sub>) [15] and tetragonal (α-WO<sub>3</sub>) [16, 17]. WO<sub>3</sub> changes in shape depending on temperature, becoming tetragonal above 740 °C, orthorhombic between 330 and 740 °C, monoclinic I between 17 and 330 °C, triclinic between –43 and 17 °C, and monoclinic II below –43 °C [18].

✉ Evan T. Salim  
evan\_tarq@yahoo.com; evan.t.salim@uotechnology.edu.iq

<sup>1</sup> Applied Science Department, University of Technology-Iraq, Baghdad 10066, Iraq

Due to its unusual physicochemical characteristics, it has the potential to be used in a variety of technical domains, including lithium-ion batteries [19–21], photocatalysts, solar energy devices [22, 23], smart windows, electronic information displays and electrochromic devices [24–30].

While  $\text{WO}_3$ , ZnO and SnO are commonly employed in sensor gas applications, tungsten in particular can detect hazardous and harmful gases such as  $\text{NO}_2$ ,  $\text{NH}_3$ , acetone [22, 31], carbon monoxide,  $\text{H}_2\text{S}$  and hydrocarbons such as benzene and methane [32–34]. However,  $\text{WO}_3$  is scarce and it is vital to produce it because of price rises and export limitations imposed by manufacturing countries that influence its availability [35].

The extremely common semiconductor metal oxides used in optoelectronic devices include  $\text{WO}_3$ ,  $\text{MoO}_3$ ,  $\text{SnO}_2$ ,  $\text{TiO}_2$  and ZnO. Surprisingly, among the total,  $\text{WO}_3$  is used in many electronic devices because of its tunable properties of high thermal stability, visible range optical absorption, surface morphology and chemical composition [36, 37].

Due to their new physical and chemical characteristics that differ fundamentally from the comparable bulk material, metal oxide nanoparticles are frequently employed as functional components in sensing, catalysis, optoelectronics and other fields [22, 38–41]. Nanotungsten has been manufactured in a variety of forms for industrial use, including nanoflowers, nanowires, nanoparticles, nanorods and nanosheets [32, 42–48]. It was formed from a variety of techniques, including spray pyrolysis, electrodeposition, anodization, sol–gel and hydrothermal processes [49–53]. Pulsed laser ablation in liquid (PLAL) is a method in which a target material is submerged in a vessel containing liquid. Liquid-phase pulsed laser ablation (LPPLA) is the same as PLAL, and this approach is not only easier to use and less expensive, but it also does not result in the generation of any undesired reaction products [54]. Pulsed laser ablation in liquid is one of the most useful ways for creating novel materials. Ablation of metal targets in liquids produced colloidal solutions containing NPs has been described. Because of their superior photochemical and photophysical capabilities as compared to bulk, metal NPs are projected to be employed as functional materials [55, 56]. Several factors, including laser intensity, wavelength, pulse width, ablation time and liquid media type, may all play an essential role in determining the product characteristics in the PLAL process [57]. This study has successfully produced  $\text{WO}_3$  NPs in water using an ND: YAG laser with a 38.21–89.11  $\text{J}/\text{cm}^2$  laser fluence. Researchers previously investigated the  $\text{WO}_3$  NPs produced using chemical methods and pulse lasers under various conditions. Hwaidi et.al reported the “Tuning Structural and Optical Properties of  $\text{WO}_3$  NPs Thin Films by the Fluency of Laser Pulses”. They successfully prepared tungsten oxide thin films by the laser pulse deposition (PLD). Results indicate that when laser fluence rises,

the film’s structural and optical characteristics improve as a result of increased crystallization and film growth [58, 59].

Majid Fakhari et.al created  $\text{WO}_3$  NPs using a Q-switched Nd:YAG laser on a tungsten plate submerged in water at varied laser fluencies. The results show that increasing laser fluence ranges from 13 to 23  $\text{J}/\text{cm}^2$ . Because of quantum confinement induced by particle size expansion, the particle’s energy band gap narrowed from 3.6 to 3.2 [60].

Breedon et.al, reported the “Synthesis of Nanostructured Tungsten Oxide Thin Films: A Simple, Controllable, Inexpensive, Aqueous Sol–Gel Method.” They propose a methodical analysis illustrating a novel technique for spin coating to create anhydrous and hydrated nanostructured tungsten oxide thin films. Results demonstrate the ability of these nanostructures to be converted into anhydrous, partly or completely hydrated tungsten oxides. The potential for  $\text{NO}_2$  sensing has been evaluated, and it was discovered that annealed tungsten oxide coatings are very sensitive to low  $\text{NO}_2$  concentrations [61, 62]

In this study, we discuss the impact of laser fluence on the morphological, structural and optical characteristics of colloidal  $\text{WO}_3$  NPs produced by laser ablation of W targets in water without the use of a catalyst. The  $\text{WO}_3$  NPs were fully characterized by using, UV–Vis spectroscopy, PL spectroscopy, XRD, SEM, EDX and TEM.

In this work, we describe the synthesis of tungsten oxide nanoparticles from a tungsten target in distilled water with the intention of examining how the laser fluence affects the characteristics of the generated nanoparticles. The ultimate objective is to generate nanometer-sized particles appropriate for constructing a nanostructured material with a very high surface-to-volume ratio and physical attributes suited for the applications indicated above.

## Experimental work

Tungsten oxide nanoparticles were created by laser ablation of a metal tungsten target in distilled water. The tungsten target was cleaned before immersion and irradiation by dipping it in acetone and washing it in pure water. The target disk was placed on an off-axis rotating target holder and submerged in distilled water in the ablation vessel. At rest, the water level was 3 mm over the objective. The ablation was performed using the fundamental (1064 nm) of an ND: YAG laser at a repetition rate of 1 Hz and a pulse width of 15 ns, with fluencies of 38.21, 50.95, 63.69, 76.43, and 89.11  $\text{J}/\text{cm}^2$ . These samples were prepared at the same number of laser pulses (200 pulses). We measured the laser energy per pulse as well as the beam spot area to calculate the laser fluence on the target, which had a spot size of around 1 mm. Figure 1 depicts a schematic representation of the pulsed laser ablation in liquid PLAL

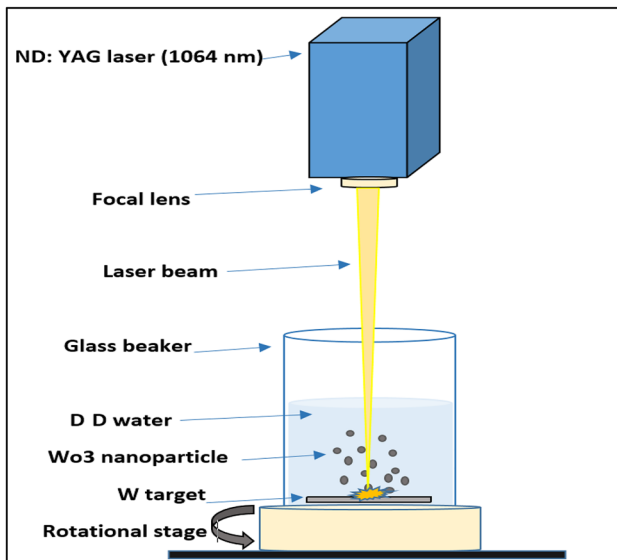
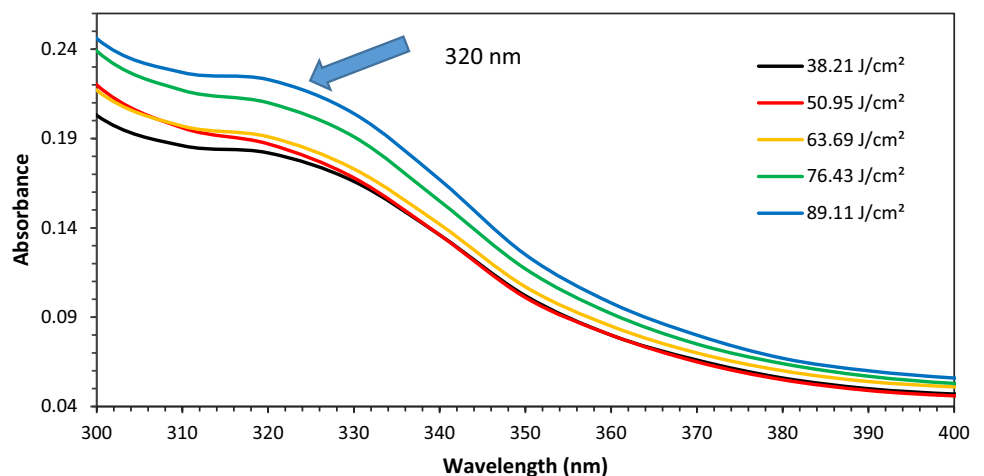


**Fig. 1** Schematic diagram of the PLAL used to synthesis WO<sub>3</sub> NPs

system utilized in this investigation. A UV–Vis double-beam spectrophotometer was used to evaluate the optical absorbance of the colloidal nanoparticle’s solution (Shimadzu UV-1800). At room temperature, with an excitation source of 325 nm wavelength, the PL emission spectra of WO<sub>3</sub> NPs produced at various laser fluence were recorded. Shimadzu’s X-ray diffractometer, model number XRD-6000, was used to take XRD measurements in order to analyze the structural characteristics of WO<sub>3</sub> NPs placed on silicon substrate. The structure and particle size of WO<sub>3</sub> NPs were studied using FESEM (T-scan Vega III Czech), and the elemental composition was analyzed using an EDX coupled with FESEM. TEM type (CM10 pw6020, Philips, Germany) was used to investigate the shape and size of WO<sub>3</sub> NPs.

**Fig. 2** UV–Vis absorption of colloidal WO<sub>3</sub> NPs at different laser fluencies



## Results and discussion

Figure 2 depicts the UV–Vis absorption spectrum of a fluid containing WO<sub>3</sub> nanoparticles at various laser fluence. The optical absorption properties of WO<sub>3</sub> NPs colloids formed at varied fluence exhibit little variation, which may be attributable to morphological similarities. These spectra are displayed in the wavelength range of 280–500 nm since higher wavelengths did not reflect unique information. The surface plasmon or exciton absorption of WO<sub>3</sub> NPs or tungsten W NPs, respectively, may be responsible for the observed absorption peaks [63–66]. It is obvious that when laser fluence increases, the absorption rises as a result of an increase in the particle concentration. Surface plasmon resonance SPR peak was seen at 320 nm due to the quantum size effect. The absorption in all samples drops off significantly beyond this wavelength [67–69]. It is well known that inter-band transition absorption is sensitive to particle density and does not alter much with particle size. As a result, absorption measurements at the wavelength of the interband transition are used to calculate the density of nanoparticles and clusters in solution [70, 71].

Optical absorption band gap follows a power law when incident photon energy greater than the band gap and above the exponential [72–75]:

$$(\alpha h\nu) = \beta(h\nu - E_g)^n \tag{1}$$

where  $E_g$  is the optical bandgap,  $\alpha$  is the absorption coefficient,  $n$  is an exponent,  $\beta$  is the edge with parameter and  $h\nu$  is the incident photon energy. As laser fluence increases from 38.21 to 89.11 J/cm<sup>2</sup>, the optical energy gap of WO<sub>3</sub> NPs decreases from 3.1 to 3.02 eV as illustrated in Fig. 3 due to the increase in the particle size and due to the enhanced crystallization [76, 77].

The influence of particle size on the band gap can be attributed to the so-called quantum confinement (QC) effect

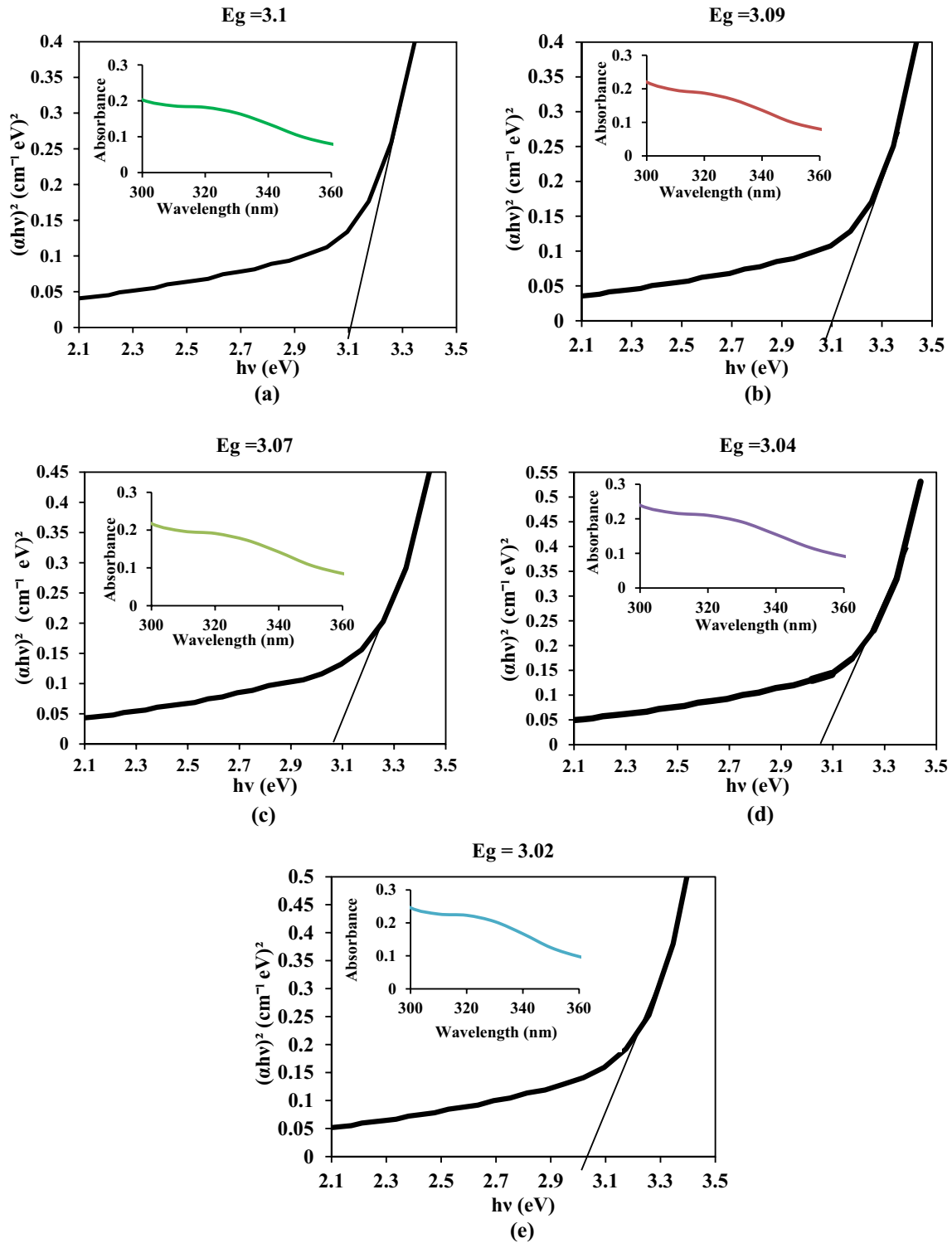


**Fig. 3**  $WO_3$  energy gap and absorption spectra using various laser fluencies, **a** 38.21 J/cm<sup>2</sup>, **b** 50.95 J/cm<sup>2</sup>, **c** 63.69 J/cm<sup>2</sup>, **d** 76.43 J/cm<sup>2</sup>, **e** 89.11 J/cm<sup>2</sup>

divided into two regimes: the so-called strong and weak. In strong QC, nanocrystal size is smaller than the Bohr radius; therefore, the electron wave functions directly change. This causes the bandgap significantly to modify. In weak QC, nanocrystal size is larger than the Bohr radius, so an indirect perturbation in the electron wave function due to Coulomb effects occurs that causes a relatively smaller shift in the bandgap. Here it can be observed that variations of particle size strongly affect the band gap energies. Thus, it seems strong QC effect has occurred [78].

Figure 4 shows the photoluminescence (PL) emission spectra of the WO<sub>3</sub> samples prepared at various laser fluence. At room temperature, photoluminescence (PL) spectroscopy is a very beneficial tool which can support in revealing the efficiency of charge carrier trapping, the energy band structures, information about surface oxygen vacancies, imperfections and impurity levels in the materials, immigration and transfer of the electrons/holes in the nanomaterials [79, 80]. PL spectra were acquired using excitation wavelengths of 325 nm. It observed the photoluminescence of 38.21 J/cm<sup>2</sup> has an emission peak centered at 404 nm corresponding to 3.06 eV. PL emission peak behaves a redshift toward a longer wavelength range (404–413 nm) (3.06–3 eV) was noticed after increasing the laser fluence from 38.21 to 89.11 J/cm<sup>2</sup>. With the increase in the laser fluence, the position of the peak has changed accordingly and the position of the peak is dependent on the band structure and size of nanoparticles (NPs). UV emission with a central wavelength of 404 nm might indicate the existence of defects and oxygen vacancies [78, 81, 82]. Increasing the laser fluence led to the increase in the particle size with the increase in the intensity of PL emission because larger NPs would possess more oxygen vacancies or defects [78, 82]. The UV–Vis data of energy gap estimated were slightly

**Table 1** Optical band gap, Emission peak and band gap energy of WO<sub>3</sub> NPs prepared at versus laser fluencies

Laser fluence (J/cm <sup>2</sup> )	UV–Vis Energy gap (eV)	PL	
		Emission peak wavelength (nm)	Band gap energy (eV)
38.21	3.1	402	3.08
50.95	3.09	406	3.05
63.69	3.07	409	3.03
76.43	3.04	411	3.01
89.11	3.02	413	3

larger than that determined from PL. Table 1 displays the predicted energy gap from PL and UV–Vis data as a function of laser fluencies. The table shows a decrease in the energy gap with increasing laser fluence, which indicates an increase in particle size with increasing laser fluence. These results match the results of UV–Vis.

XRD tests were carried out to study the crystal structure and preferred orientation of the crystallites. For X-ray diffraction (XRD) analysis, a number of droplets of transparent colloidal samples generated at various laser fluence were positioned on silicon substrates with dimensions of 1 cm by 1 cm and 1 mm thick and allowed to dry naturally at a range of temperatures from 50 to 70 °C. Figure 5 displays the XRD patterns of the samples created by laser fluencies of 38.21, 50.95, 63.69, 76.43 and 89.11 J/cm<sup>2</sup>. It has been shown that samples' XRD peaks differ from W target peaks. It may be inferred that ablated W and water molecules engaged in chemical and physical reactions that resulted in the creation of WO<sub>3</sub> NPs in the water environment [83–85]. Four peaks have been found at 2θ = 25.5°, 39.72°, 43.68° and

**Fig. 4** PL emission spectra of samples prepared at different laser fluence recorded at 325 nm excitation wavelength

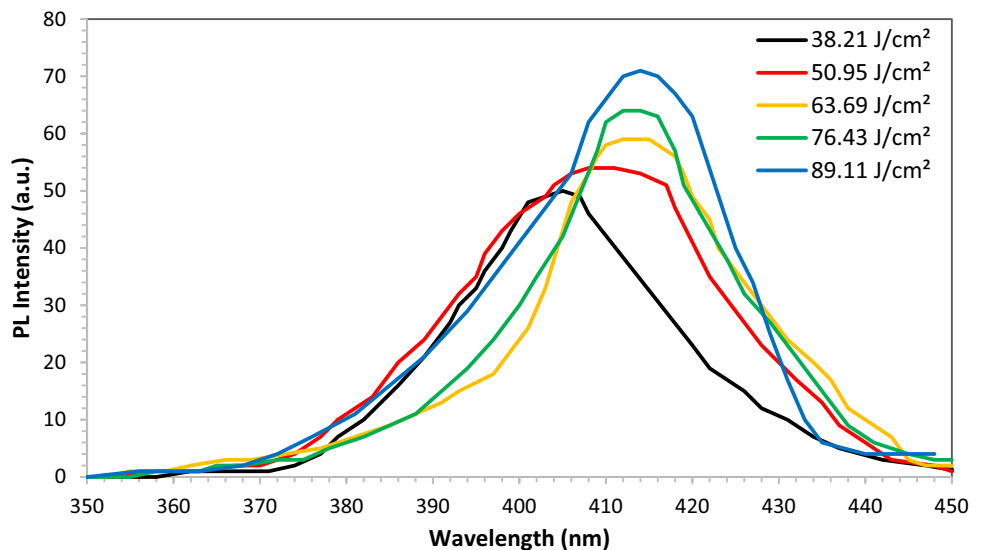
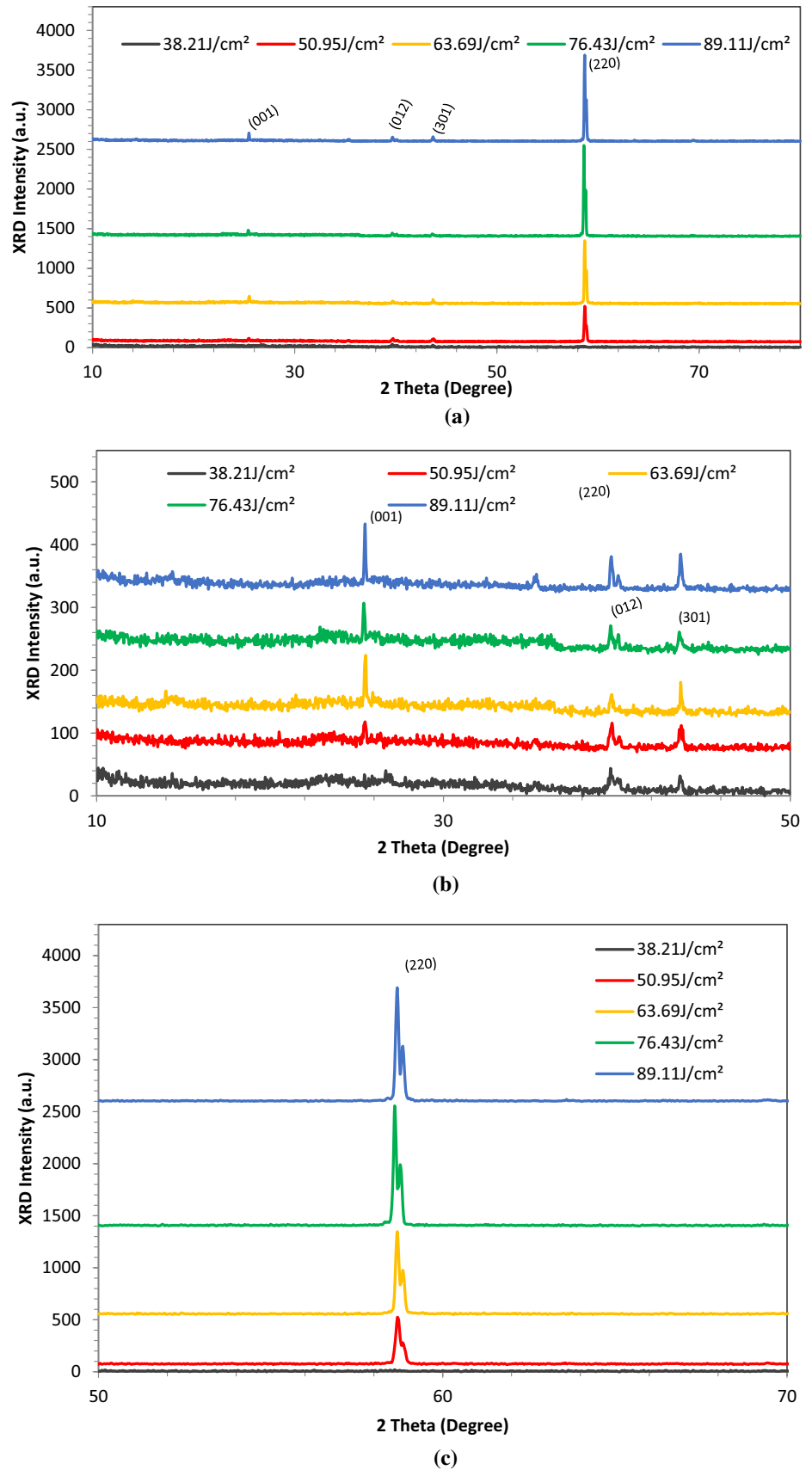


**Fig. 5** **a** XRD pattern of a  $\text{WO}_3$  NPs prepared at different laser fluencies. **b** Zoom graph of the 10–45 region XRD patterns of  $\text{WO}_3$  samples. **c** Zoom graph of the 50–70 region XRD patterns of  $\text{WO}_3$  samples





58.77 corresponding to (110), (012), (301) and (220) planes, respectively, according to (JCPDS # 33–1387) (JCPDS # 89–1287) (pdf number # 75–2186). With an increase in the ablation energy, the peak’s intensity and sharpness start to rise. WO<sub>3</sub> NPs appear a sharp peak at 2θ=58.77 correspond to (220) plane and exhibited preferential orientation along (220) plane of all the samples, as shown in Fig. 5. By increasing the laser fluencies from 38.11 to 76,43 J/cm<sup>2</sup>, the intensity of (220) diffraction peak increases due to the increased crystallization [86]. As the laser fluencies increase to 89. 11 J/cm<sup>2</sup>, we show a decrease in the (220) diffraction peak intensity and the peak intensity begins to decrease due to decreasing the structure crystallization [87, 88]. No shift in XRD peak position was noticed with increasing the laser fluence.

Figure 5 shows a—XRD pattern of a WO<sub>3</sub> NPs prepared at different laser fluencies, b—zoom graph of the 10–45 region XRD patterns of WO<sub>3</sub> samples and c—zoom graph of the 50–70 region XRD patterns of WO<sub>3</sub> samples [the Scherrer formula is used to calculate the size of crystallites] [89–92].

$$D = k\lambda / (\beta \cos \theta) \tag{2}$$

where λ is X-ray wavelength, β is the full width at the half maximum and k is constant 0.89 < k < 1 change with Miller indices and crystallite shape, but is frequently close to 0.94 and θ is the diffraction angle. Table 2 shows the relationship between crystallite sizes of WO<sub>3</sub> was calculated for (220) plane have been found at 2θ=58.7° and laser fluence. It is observed that the crystallite size increases from 38.08 to 71.65 nm as the laser fluence rises from 38.21 to 89.11 J/cm<sup>2</sup>. Where the values of the crystallite size are found that 38.08, 47.92, 65.79, 71.65 and 72.37 nm corresponding to the laser fluence of 38.21, 50.95, 63.69, 76.43 and 89.11 J/cm<sup>2</sup>, respectively.

It is found 38.08, 47.92, 65.79, 71.65 and 72.37 nm corresponding to the laser fluence of 38.21, 50.95, 63.69, 76.43 and 89.11 J/cm<sup>2</sup>, respectively.

FESEM was used to examine the morphology of the WO<sub>3</sub> NPs as shown in Fig. 6 which shows for the five samples a, b, c, d and e produced using various laser fluencies 38.21, 50.95, 63.69, 76.43 and 89.11 J/cm<sup>2</sup>, respectively.

These samples were prepared by the deposition of the WO<sub>3</sub> colloidal using a drop cast method on the quartz substrate. FESEM pictures revealed that the crystallization of WO<sub>3</sub> NPs increased with increasing laser fluence due to increased grain size. The WO<sub>3</sub> NPs have been seen to aggregate and agglomerate. Increased laser fluence causes an increase in particle density in liquid due to increased ablated volume. Raising the laser fluence causes the creation of tiny WO<sub>3</sub> droplets, which are fractured by their contact with the incoming laser beam, followed by fast quenching, resulting in the synthesis of bigger nanoparticles, therefore lowering the interfacial distances between them [93, 94]. Particle agglomerate was showed as the laser fluence above 63.69 J/cm<sup>2</sup>. NPs can be observed to be spherical and attached to one another. Further increasing in the laser fluence leads to the formation of larger spherical particle structure.

The elemental composition of the samples was investigated using EDX analysis. Figure 7 depicts the EDS spectra of samples prepared at various laser fluencies. All of the samples’ spectra show the presence of W and O elements. The Au signals found in the EDS spectra are attributable to the gold coating on samples prior to EDX examination [95]. EDX spectra show very high W peak may be as a result of superposition of the X-ray [96, 97]. EDX measurements explain that the laser fluence increases with the increase in the concentration of the ratio O/W as a result of oxidation processes.

Table 3 presents the effect of laser fluence on [O]/[W] wt% ratio, We can see from the table that the ratio of [O]/[W] wt% increases when the fluence of the laser is increased, and the values of [O]/[W] wt% ratio were 0.29, 0.40, 0.43, 0.93 and 0.99 for colloidal prepared at laser fluence of 38.21, 50.95, 63.69, 76.43 and 89.11 J/cm<sup>2</sup>, respectively.

Based on EDX data, the best values of [O]/[W] wt% ratio for colloidal were found for sample at 76.43 and 89.11 J/cm<sup>2</sup>.

While the proportion of oxygen has increased, this suggests that the atom is more likely to receive an electron to achieve a stable state [86], as shown in Fig. 8.

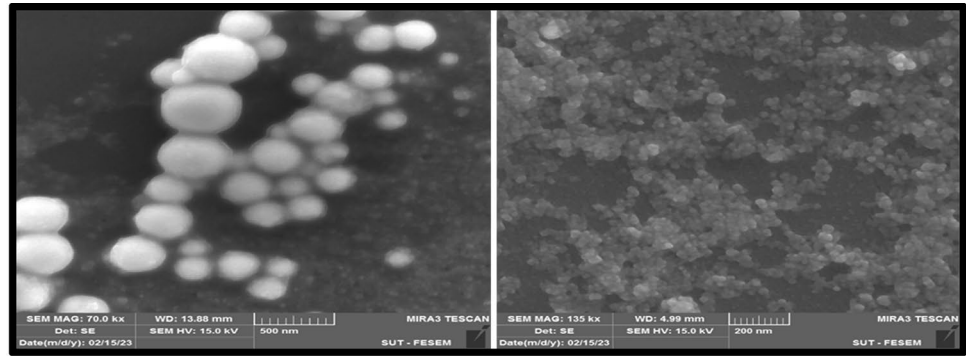
The spherical nanoparticles were created using a 1064 nm Nd:YAG laser at various fluencies between 38.21 and 89.11 J/cm<sup>2</sup> according to TEM pictures.

Figure 9 shows TEM and particle size histogram for wo3 nanoparticles prepared with different laser fluencies a

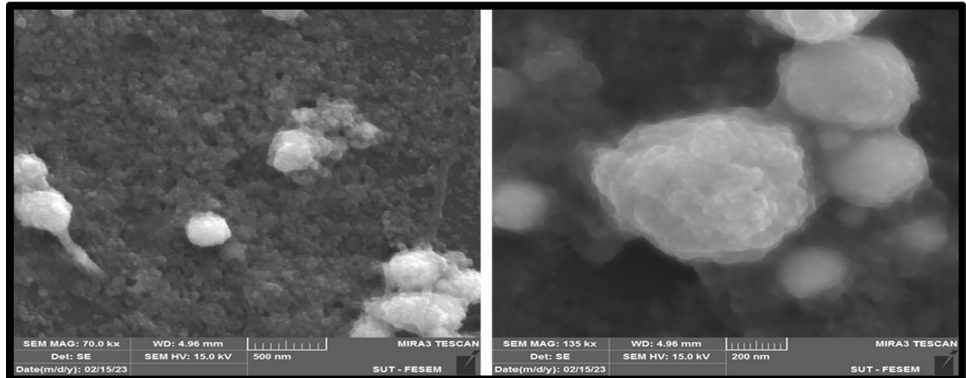
**Table 2** Average crystallite size of WO<sub>3</sub> obtained from XRD at different laser fluencies

No	Laser fluence (J/cm <sup>2</sup> )	2θ (deg)	2θ/2	klh	FWHM	D <sub>XRD</sub> (nm)
1	38.21	58.7°	29.24	220	0.19	38.08
2	50.95	58.7°	29.33	220	0.151	47.92
3	63.69	58.7°	29.33	220	0.11	65.79
4	76.43	58.7°	29.295	220	0.101	71.65
5	89.11	58.7°	29.295	220	0.1	72.37

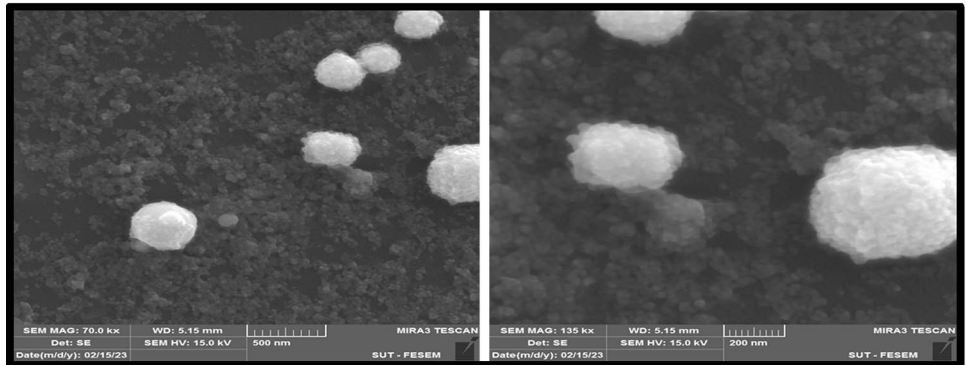
**Fig. 6** FESEM images of  $\text{WO}_3$  NPs synthesized at different laser fluencies **a**  $38.21 \text{ J/cm}^2$ , **b**  $50.95 \text{ J/cm}^2$ , **c**  $63.69 \text{ J/cm}^2$ , **d**  $76.43 \text{ J/cm}^2$ , **e**  $89.11 \text{ J/cm}^2$



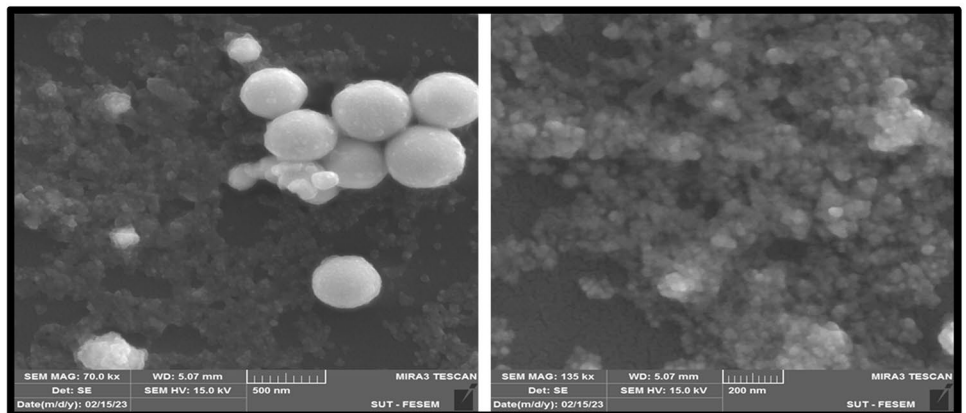
(a)



(b)



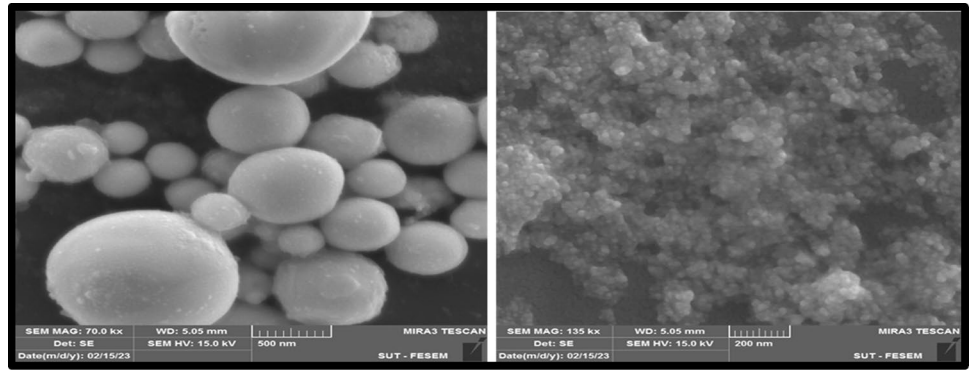
(c)



(d)

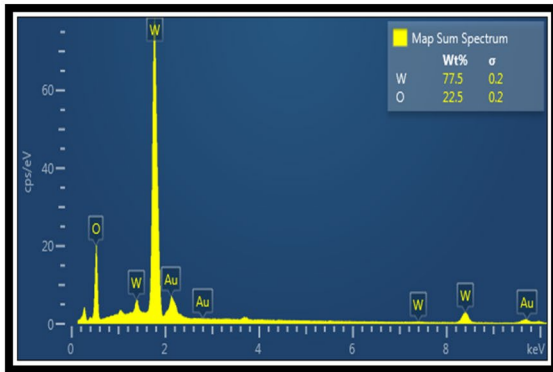


Fig. 6 (continued)

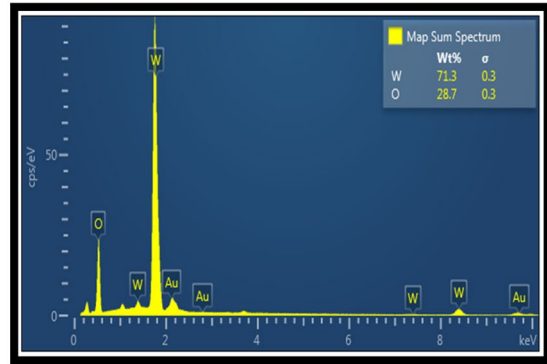


(e)

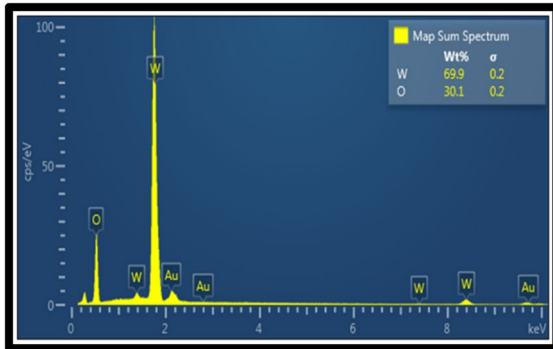
(a)



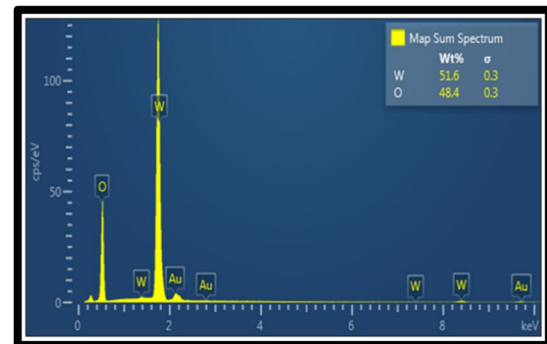
(b)



(c)



(d)



(e)

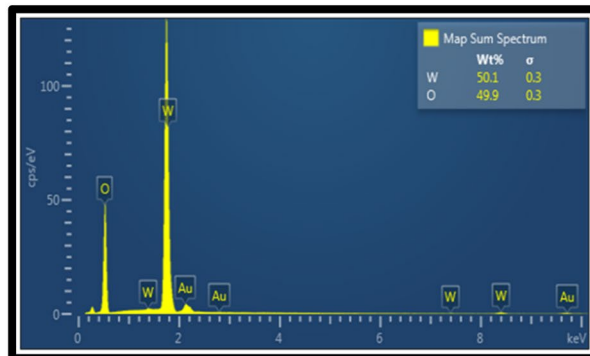
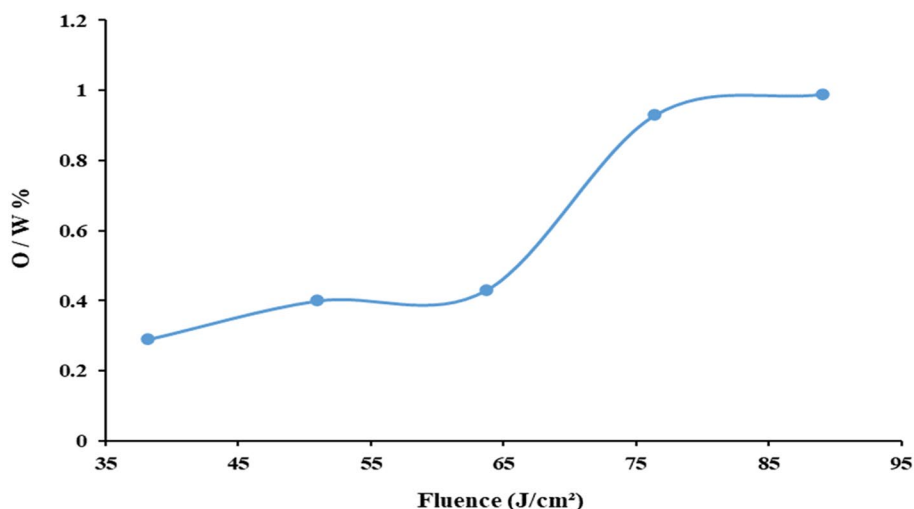


Fig. 7 EDX spectra of wo3 NPs synthesized at different laser fluencies a 38.21 J/cm<sup>2</sup>, b 50.95 J/cm<sup>2</sup>, c 63.69 J/cm<sup>2</sup>, d 76.43 J/cm<sup>2</sup>, e 89.11 J/cm<sup>2</sup>

**Fig. 8** Concentration of the ratio O/W of WO<sub>3</sub> NPs at the fluence of 38.21, 50.95, 63.69, 76.43 and 89.11 (J/cm<sup>2</sup>)



38.21 J/cm<sup>2</sup>, b 50.95 J/cm<sup>2</sup>, c 63.69 J/cm<sup>2</sup>, d 76.43 J/cm<sup>2</sup> and e 89.11 J/cm<sup>2</sup>. Small, spherical particles with low concentrations at low laser fluence were seen in TEM pictures. With increasing laser fluence, particle size and concentration rose from 6 to 33 nm. The sample generated with 89.11 J/cm<sup>2</sup> laser fluence provided very well-defined spherical forms with greater concentration, as shown in Fig. 9, as well as a high agglomeration rate, as demonstrated in the average size histograms in Table 4, where the table shows an increase in average particle size in TEM pictures as the laser fluence rises from 38.21 to 89.11 J/cm<sup>2</sup>. This result agrees with the results of previous studies [98–102]. This may be attributed to the elevated probability of collision between the vapor atoms and ions within the plasma plume leading to larger-sized particles as mentioned elsewhere [103–105]. This result agrees with SEM result mentioned earlier.

## Conclusion

WO<sub>3</sub> NPs have been successfully synthesized by nanosecond pulsed laser ablation in liquid. FESEM observed the formation of a spherical shape and an increase in the size

distribution due to increasing laser fluence. The absorption spectrum demonstrates the edge of NPs performs around ~320 nm, which is blueshifted from the absorption edge of bulk material. The values of the obtained energy gap change from 3.1 to 3.02 eV according to the fluence of laser. TEM result shows the particle size and concentration of wO<sub>3</sub> increased from 6 to 33 nm with increasing laser fluence. All of the previous findings support the significant potential of laser ablation in liquids as a viable technology for producing tungsten oxide nanoparticle colloids without the need of chemical reagents in a simple, streamlined and cost-effective manner. This experimental work also aims to show how varying the laser fluence may be used to control on the size of WO<sub>3</sub> nanoparticles in this range of ablation parameters.

There are a few limitations in this study, it requires the speed of conducting examinations of the samples in order for the results to be accurate.

It is expected that there will be many future studies on the effect of the rest of the laser parameters (wavelength, number of laser pulses, etc.) on the optical, structural and morphology properties of WO<sub>3</sub> NPs produced by pulsed laser ablation in liquid environment because of the importance of this material in many applications as mentioned earlier and also this method (PLAL) is easy to use and less expensive and

**Table 3** [O]/[W] ratio and stoichiometric percentage as function of laser fluence

Laser fluence (J/cm <sup>2</sup> )	W %	O %	O/W
38.21	77.5	22.5	0.29
50.95	71.3	28.7	0.40
63.69	69.9	30.1	0.43
76.43	51.6	48.4	0.93
89.11	50.1	49.9	0.99

**Table 4** Average particle size using different laser fluencies

Laser fluence (J/cm <sup>2</sup> )	Average particle size (nm)
38.21	6
50.95	14
63.69	16
76.43	28
89.11	33

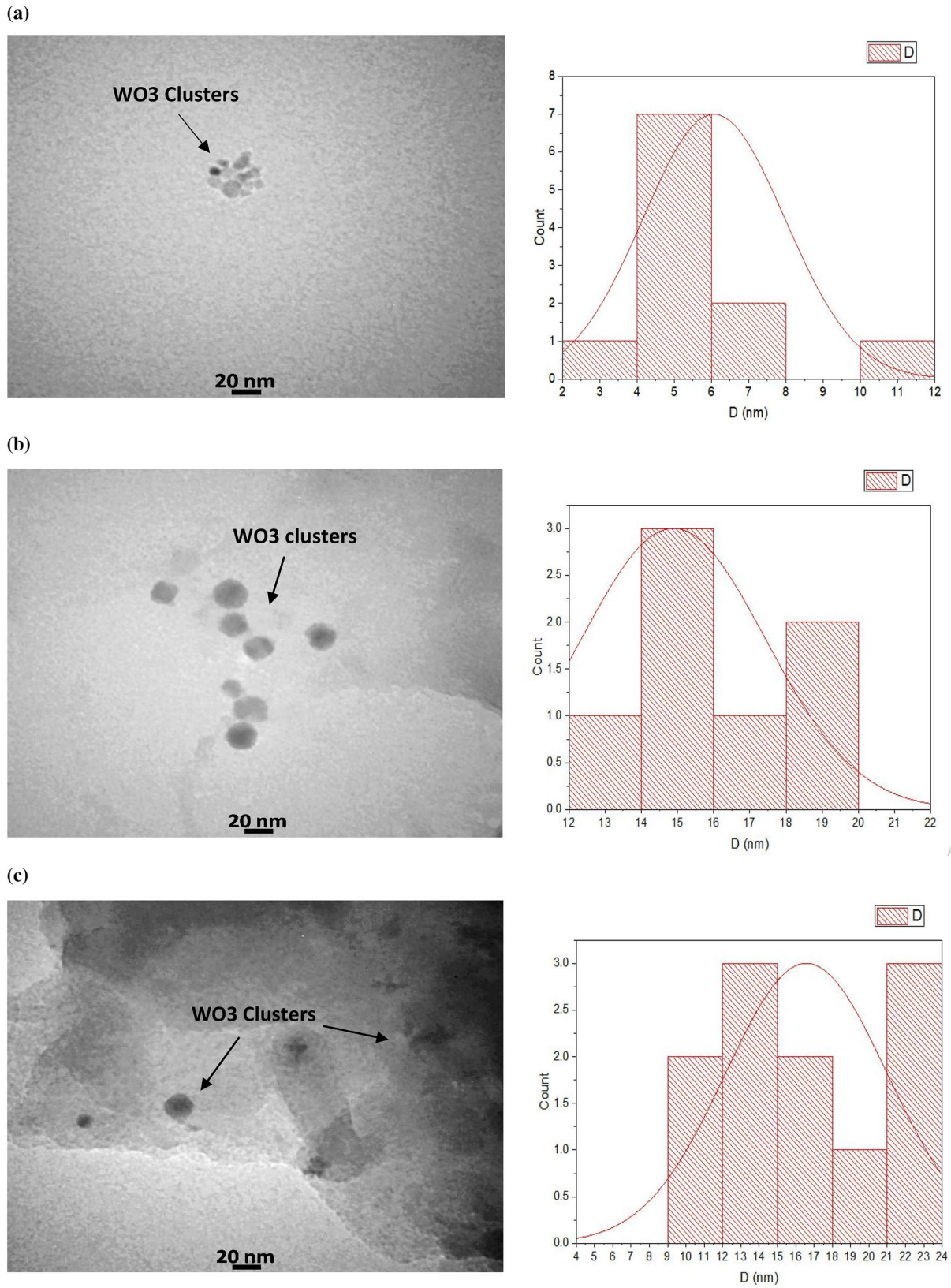
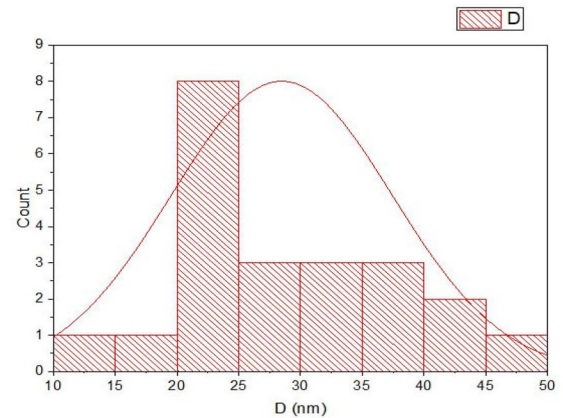
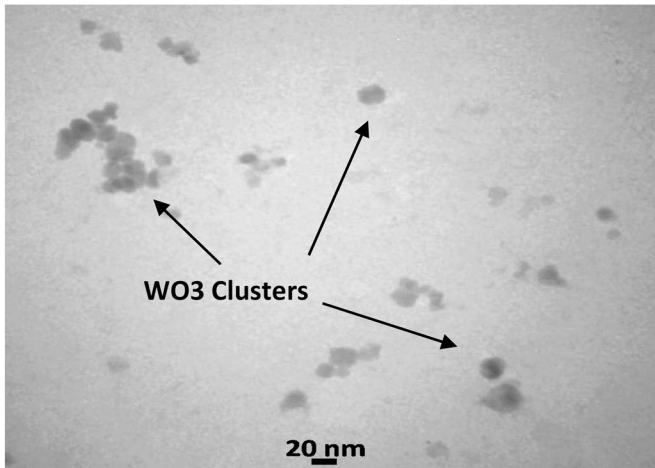


**Fig. 9** TEM and particle size histogram for wo3 nanoparticles prepared with different laser fluencies **a** 38.21 J/cm<sup>2</sup>, **b** 50.95 J/cm<sup>2</sup>, **c** 63.69 J/cm<sup>2</sup>, **d** 76.43 J/cm<sup>2</sup>, **e** 89.11 J/cm<sup>2</sup>

(d)



(e)

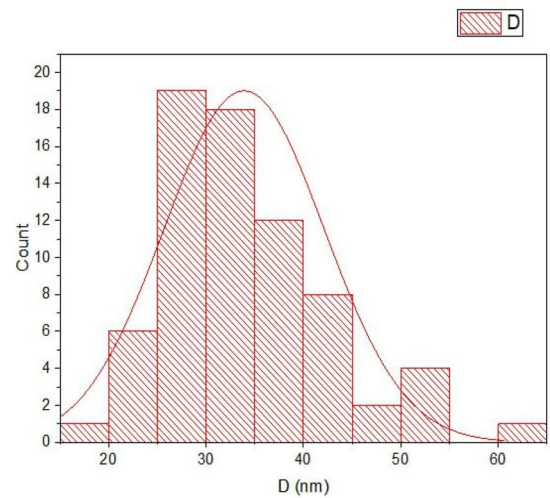
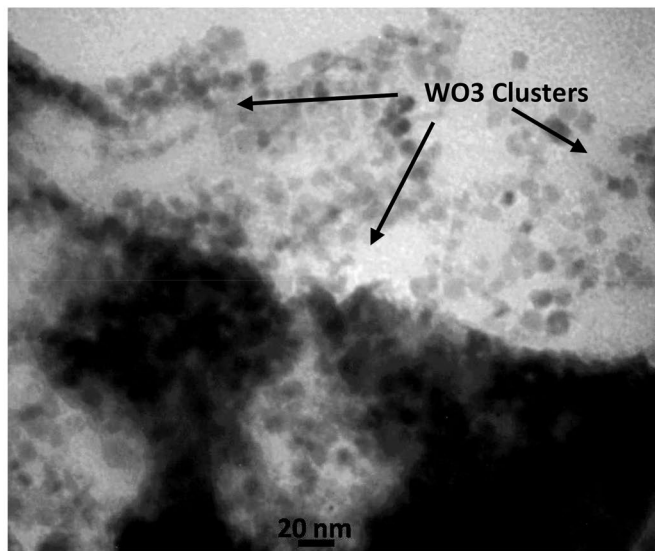


Fig. 9 (continued)

does not result in the generation of any undesired reaction products.

**Acknowledgements** The authors would like to thank the University of Technology for the logistic support this work.

**Author contributions** MSM and ETS were involved in conceptualization, investigation and data curation; MSM, ETS and JAS assisted with the methodology and formal analysis; ETS and JAS were responsible for validation, resources, visualization, supervision and project administration; MSM participated in writing—original draft preparation; and ETS took part in writing—reviewing and editing. All authors have read and agreed to the published version of the manuscript.

**Funding** No funding.

**Data availability** The datasets used and/or analyzed during the current study is available from the corresponding authors “Maryam S. Muhsin, Evan T. Salim” on reasonable request.

#### Declarations

**Conflict of interest** We hereby confirm that the authors have no conflict of interest and the disclosure made for this manuscript is complete and correct to the best of our information and belief. We agree that if we become aware of any information that might indicate that this disclosure is inaccurate or that we have not complied with the conflict of interest policy, we will notify the journal immediately. The authors have declared that no competing interests exist.



## References

- C. Chacón, M.R. Pérez, G. Oskam, G.R. Gattorno, Synthesis and characterization of WO<sub>3</sub> polymorphs: monoclinic, orthorhombic and hexagonal structures. *J. Mater. Sci. Mater. Electron.* **26**, 5526–553 (2015)
- E.T. Salim, J.A. Saimon, M.K. Abood, M.A. Fakhri, Effect of silicon substrate type on Nb<sub>2</sub>O<sub>5</sub>/Si device performance: an answer depends on physical analysis. *Opt. Quantum Electron.* **52**(10), 463 (2020)
- R. Mukherjee, A. Kushwaha, P.P. Sahay, Spray-deposited nanocrystalline WO<sub>3</sub> thin films prepared using tungsten hexachloride dissolved in NN dimethyl formamide and influence of in doping on their electron. *Mater. Lett.* **10**, 401–410 (2014)
- J. Li, X. Liu, J. Cui, J. Sun, Hydrothermal synthesis of self-assembled hierarchical tungsten oxides hollow spheres and their gas sensing properties. *ACS Appl. Mater. Interfaces.* **7**, 10108–10114 (2015)
- M.A. Fakhri, R.A. Ismail, A.K. Abass, L.Z. Mohammed, F.H. Alsultany, U. Hashim, Synthesis of LiNbO<sub>3</sub>/SiO<sub>2</sub>/Si nanostructures layer by layer based on Mach-Zehnder modulator using pulsed laser deposition route. *Silicon* **14**, 11781–11795 (2022)
- R. Nagarjuna, S. Challagulla, P. Sahu, S. Roy, R. Ganesan, Polymerizable sol–gel synthesis of nano-crystalline WO<sub>3</sub> and its photocatalytic Cr (VI) reduction under visible light. *Adv. Powder Technol.* **28**, 3265–3273 (2017)
- A. Temmink, O. Anderson, K. Bange, H. Hantsche, X. Yu, Optical absorption of amorphous WO<sub>3</sub> and binding state of tungsten. *Thin Solid Films* **192**, 211–218 (1990)
- M.K. Abood, E.T. Salim, J.A. Saimon, Impact of substrate type on the microstructure of H-Nb<sub>2</sub>O<sub>5</sub> thin film at room temperature. *Int. J. Nanoelectron. Mater.* **11**, 55–64 (2018)
- G.R. Bamwenda, H. Arakawa, The visible light induced photocatalytic activity of tungsten trioxide powders. *Appl. Catal. A Gen.* **210**, 181–91 (2001)
- F. Cora, M.G. Stachitti, C.R. Catlow, C. Rodriguez, Transition metal oxide chemistry: electronic structure study of WO<sub>3</sub>, ReO<sub>3</sub> and NaWO<sub>3</sub>. *J. Phys. Chem. B* **101**, 3945–52 (1997)
- S.A. Naayi, A.I. Hassan, E.T. Salim, FTIR and X-ray diffraction analysis of Al<sub>2</sub>O<sub>3</sub> nanostructured thin film prepared at low temperature using spray pyrolysis method. *Int. J. Nanoelectron. Mater.* **11**, 1–6 (2018)
- S. Tanisaki, Crystal structure of monoclinic tungsten trioxide at room temperature. *J. Phys. Soc. Jpn.* **15**, 573–581 (1960)
- P.M. Woodward, A.W. Sleight, T. Vogt, Structure refinement of triclinic tungsten trioxide. *J. Phys. Chem. Solids* **56**, 1305–15 (1995)
- M.A. Fakhri, N.H. Numan, Q.Q. Mohammed, M.S. Abdulla, O.S. Hassan, S.A. Abduljabar, A.A. Ahmed, Responsivity and response time of nano silver oxide on silicon heterojunction detector. *Int. J. Nanoelectron. Mater.* **11**, 65–72 (2018)
- C. Kratky, H.P. Isenring, J. Dunitz, Methylpyrochlorophyllide a monohydrate monoetherate. *Acta Crystallogr. Sect. B Struct. Crystallogr. Cryst. Chem.* **33**, 547–9 (1977)
- W.L. Kehl, R.G. Hay, D. Wahl, The structure of tetragonal tungsten trioxide. *J. Appl. Phys.* **23**, 212–215 (1952)
- M.A. Fakhri, N.H. Numan, Q.Q. Mohammed, M.S. Abdulla, O.S. Hassan, S.A. Abduljabar, A.A. Ahmed, Responsivity and response time of nano silver oxide on silicon heterojunction detector. *Int. J. Nanoelectron. Mater.* **11**, 109–114 (2018)
- H. Zheng, J.Z. Ou, M.S. Strano, R.B. Kaner, A. Mitchell, K. Kalantar-zadeh, Nanostructured tungsten oxide-properties, synthesis, and applications. *Adv. Funct. Mater.* **21**, 2175–96 (2011)
- S. Komaba, N. Kumagai, K. Kato, H. Yashiro, Hydrothermal synthesis of hexagonal tungsten trioxide from Li<sub>2</sub>WO<sub>4</sub> solution and electrochemical lithium intercalation into the oxide. *Solid State Ionics* **135**, 193–197 (2000)
- M.A. Fakhri, Y. Al-Douri, A. Bouhemadou, M. Ameri, Structural and optical properties of nanophotonic LiNbO<sub>3</sub> under stirrer time effect. *J. Opt. Commun.* **39**(3), 297–306 (2017)
- S. Salmaoui, F. Sediri, N. Gharbi, C. Perruchot, S. Aeiayah, I.A. Rutkowska, P.J. Kulesza, M. Jouini, Hexagonal nanorods of tungsten trioxide: synthesis, structure, electrochemical properties and activity as supporting material in electrocatalysis. *Appl. Surf. Sci.* **257**, 8223–8229 (2011)
- J. Li, X. Liu, J. Cui, J. Sun, Hydrothermal synthesis of self-assembled hierarchical tungsten oxides hollow spheres and their gas sensing properties. *ACS Appl. Mater. Interfaces.* **7**, 10108–10114 (2015)
- M.A. Fakhri, E.T. Salim, A.W. Abdulwahhab, U. Hashim, Z.T. Salim, Optical properties of micro and nano LiNbO<sub>3</sub> thin film prepared by spin coating. *Opt. Laser Technol.* **103**, 226–232 (2018)
- H.J. Chen, N.S. Xu, S.Z. Deng, D.Y. Lu, Z.L. Li, J. Zhou, Gasochromic effect and relative mechanism of WO<sub>3</sub> nanowire films. *J. Chem. Nanotechnol.* **18**, 205701 (2007)
- Y. Hattori, S. Nomura, S. Mukasa, H. Toyota, T. Inoue, T. Kasahara, *J. Alloys, J. Alloys Comp.* **560**, 105–110 (2013)
- M.A. Fakhri, E.T. Salim, M.H.A. Wahid, U. Hashim, Z.T. Salim, Optical investigations and optical constant of nano lithium niobate deposited by spray pyrolysis technique with injection of Li<sub>2</sub>CO<sub>3</sub> and Nb<sub>2</sub>O<sub>5</sub> as raw materials. *J. Mater. Sci. Mater. Electron.* **29**(11), 9200–9208 (2018)
- Y.X. Qin, F. Wang, W.J. Shen, M. Hu, Mesoporous three-dimensional network of crystalline WO<sub>3</sub> nanowires for gas sensing application. *J. Alloys Comp.* **540**, 21–26 (2012)
- L. Fang, S.J. Baik, K.S. Lim, S.H. Yoo, M.S. Seo, S.J. Kang, J.W. Seo, Tunable work function of a WO<sub>x</sub> buffer layer for enhanced photocarrier collection of pin-type amorphous silicon solar cells. *Appl. Phys. Lett.* **96**, 193501 (2010)
- M.K. Abood, E.T. Salim, J.A. Saimon, Niobium pentoxide thin film prepared using simple colloidal suspension for optoelectronic application. *Int. J. Nanoelectron. Mater.* **11**(2), 127–134 (2018)
- P.J. Barczuk, A. Krolkowska, A. Lewera, K. Miecznikowski, R. Solarska, J. Augustynski, Structural and photoelectrochemical investigation of boron-modified nanostructured tungsten trioxide films. *Electrochim. Acta* **104**, 282–288 (2013)
- Y. Al-Douri, M.A. Fakhri, N. Badi, C.H. Voon, Effect of stirring time on the structural parameters of nanophotonic LiNbO<sub>3</sub> deposited by spin-coating technique. *Optik* **156**, 886–890 (2018)
- L. Wang, H. Hu, J. Xu, S. Zhu, A. Ding, C. Deng, WO<sub>3</sub> nanocubes: hydrothermal synthesis, growth mechanism, and photocatalytic performance. *J. Mater. Res.* **34**, 2955–2963 (2019)
- A. Forbes, R.M. Erasmus, Synthesis of tungsten oxide nanostructures by laser pyrolysis Bonex Wakufwa Mwakikunga \* Elias Sideras-Haddad and Gift Katumba Bathusile Masina. *Int. J. Nanopart.* **1**, 185–202 (2008)
- Y. Al-Douri, M.A. Fakhri, A. Bouhemadou, R. Khenata, M. Ameri, Stirrer time effect on optical properties of nanophotonic LiNbO<sub>3</sub>. *Mater. Chem. Phys.* **203**, 243–248 (2018)
- O. Arutanti, A.B.D. Nandiyanto, T. Ogi, F. Iskandar, T.O. Kim, K. Okuyama, Synthesis of composite WO<sub>3</sub>/TiO<sub>2</sub> nanoparticles by flame-assisted spray pyrolysis and their photocatalytic activity. *J. Alloys Compd.* **591**, 121–126 (2014)
- K. Shanmugasundaram, P. Thirunavukkarasu, M. Ramamurthy, M. Balaji, J. Chandrasekaran, Growth and characterization of jet nebulizer spray deposited n-type WO<sub>3</sub> thin films for junction diode application. *Orient. J. Chem.* **33**(5), 2484 (2017)
- M.A. Fakhri, E.T. Salim, M.H.A. Wahid, A.W. Abdulwahhab, U. Hashim, Z.T. Salim, Efficiency enhancement of optical strip

- waveguide by the effect of heat treatment. *Optik* **180**, 768–774 (2019)
38. D. Mott, J. Galkowski, L. Wang, J. Luo, C.J. Zhong, Synthesis of size-controlled and shaped copper nanoparticles. *Langmuir* **23**, 5740 (2007)
  39. M.A. Fakhri, E.T. Salim, A.W. Abdulwahhab, U. Hashim, M.A. Minshid, Z.T. Salim, The effect of annealing temperature on optical and photoluminescence properties of LiNbO<sub>3</sub>. *Surf. Rev. Lett.* **26**(10), 1950068 (2019)
  40. A. Boudiba, C. Zhang, C. Bittencourt, P. Umek, Hydrothermal synthesis of two-dimensional WO<sub>3</sub> nanostructures for NO<sub>2</sub> detection in the ppb-level. *Proced. Eng.* **47**, 228–231 (2012)
  41. Y. Hattori, S. Nomura, S. Mukasa, H. Toyota, T. Inoue, Synthesis of tungsten trioxide nanoparticles by microwave plasma in liquid and analysis of physical properties. *J. Alloys Compd.* **560**, 105–110 (2013)
  42. A.D. Faisal, R.A. Ismail, W.K. Khalef, E.T. Salim, Synthesis of ZnO nanorods on a silicon substrate via hydrothermal route for optoelectronic applications. *Opt. Quant. Electron.* **52**, 1–12 (2020)
  43. G. Leftheriotis, S. Papaefthimiou, P. Yianoulis, A. Siokou, D. Kefalas, Structural and electrochemical properties of opaque sol-gel deposited WO<sub>3</sub> layers. *Appl. Surf. Sci.* **218**, 276–281 (2003)
  44. A. Tasaso, P. Ngaotranawiwat, *Synthesis of Nano-WO<sub>3</sub> Particles with Polyethylene Glycol for Chromic Film* (Elsevier, Amsterdam, 2015)
  45. M.A. Fakhri, M.J. AbdulRazzaq, A.A. Alwahib, W.H. Muttlak, Theoretical study of a pure LinbO<sub>3</sub>/Quartz waveguide coated gold nanorods using supercontinuum laser source. *Opt. Mater.* **109**, 110363 (2020)
  46. H.A.A.A. Amir, M.A. Fakhri, A.A. Alwahib, E.T. Salim, F.H. Alsultany, U. Hashim, An investigation on GaN/porous-Si NO<sub>2</sub> gas sensor fabricated by pulsed laser ablation in liquid. *Sens. Actuators B: Chem.* **367**, 132163 (2022)
  47. F.A. Mohamed, A.I. Hassan, E.T. Salim, Meso-porous-like tungsten oxide structure: a study on some physical properties at different deposited temperatures. *Int. J. Nanoelectron. Mater.* **15**(4), 281–292 (2022)
  48. R. Hu, H. Wu, K. Hong, Synthesis and characterization of nanocrystalline tungsten oxide nanosheets in large scale. *J. Mater. Res.* **24**, 187–191 (2009)
  49. A.A. Rashid, S. Nor Hayati, C.S.D. Bien, W.Y. Lee, A.S. Muhammad, Preliminary study of WO<sub>3</sub> nanostructures produced via facile hydrothermal synthesis process for CO<sub>2</sub> sensing. *Appl. Mech. Mater.* **2013**, 37–41 (2013)
  50. M.A. Fakhri, R.A. Ismail, A.K. Abass, L.Z. Mohammed, F.H. Alsultany, U. Hashim, Synthesis of LiNbO<sub>3</sub>/SiO<sub>2</sub>/Si nanostructures layer by layer based on mach-zehnder modulator using pulsed laser deposition route. *Silicon* **14**(17), 11781–11795 (2022)
  51. B.T. Sone, J. Sithole, R. Bucher, S.N. Mlondo, J. Ramontja, S.S. Ray, E. Iwuoha, M. Maaza, Synthesis and structural characterization of tungsten trioxide nanoplatelet-containing thin films prepared by aqueous chemical growth. *Thin Solid Films* **522**, 164–170 (2012)
  52. T. Zhu, M.N. Chong, Y.W. Phuan, J.D. Ocon, E.S. Chan, Effects of electrodeposition synthesis parameters on the photoactivity of nanostructured tungsten trioxide thin films: optimisation study using response surface methodology. *J. Taiwan Inst. Chem. Eng.* **61**, 196–204 (2016)
  53. H.A.A.A. Amir, M.A. Fakhri, A.A. Alwahib, E.T. Salim, F.H. Alsultany, U. Hashim, Synthesis of gallium nitride nanostructure using pulsed laser ablation in liquid for photoelectric detector. *Mater. Sci. Semicond. Process.* **150**, 106911 (2022)
  54. Z. Jing, M. Hu, W. Wang, H. Chen, Y. Qin, NO<sub>2</sub>-sensing properties of porous WO<sub>3</sub> gas sensor based on anodized sputtered tungsten thin film. *Sens. Actuators B Chem.* **161**, 447–452 (2012)
  55. T. Tsuji, K. Iryo, Y. Nishimura, M. Tsuji, Preparation of metal colloids by a laser ablation technique in solution: influence of laser wavelength on the ablation efficiency (II). *J. Photochem. Photobiol. A Chem.* **145**, 201–207 (2001)
  56. M.A. Fakhri, E.T. Salim, M.H.A. Wahid, U. Hashim, Z.T. Salim, R.A. Ismail, Synthesis and characterization of nanostructured LiNbO<sub>3</sub> films with variation of stirring duration. *J. Mater. Sci.: Mater. Electron.* **28**(16), 11813–11822 (2017). <https://doi.org/10.1007/s10854-017-6989-0>
  57. A. Baladi, R.S. Mamooory, Investigation of different liquid media and ablation times on pulsed laser ablation synthesis of aluminum nanoparticles. *J. Appl. Surf. Sci.* **256**(24), 7559–7564 (2010)
  58. A.J. Hwaidi, N.J. Mohammed, Tuning structural and optical properties of WO<sub>3</sub> NPs thin films by the fluency of laser pulses. *Al-Mustansiriyah J. Sci.* **33**(3), 94–100 (2022)
  59. T.E. Abdulrahman, E.T. Salim, R.O. Mahdi, M.H.A. Wahid, Nb<sub>2</sub>O<sub>5</sub> nano and microspheres fabricated by laser ablation. *Adv. Nat. Sci: Nanosci. Nanotechnol.* **13**, 045006 (2022)
  60. M. Fakhari, M.J. Torkamany, S.N. Mirnia, Linear and nonlinear optical properties of WO<sub>3</sub> nanoparticles synthesized at different fluences of pulsed Nd: YAG laser. *Eur. Phys. J. Appl. Phys.* **84**(3), 30401 (2018)
  61. M. Breedon et al., Synthesis of nanostructured tungsten oxide thin films: a simple, controllable, inexpensive, aqueous sol-gel method. *Cryst. Growth Des.* **10**(1), 430–439 (2010)
  62. R.B. Fafhil, E.T. Salim, W.K. Khalef, Synthesis of LiNbO<sub>3</sub> microstructures: structural, optical, and surface morphology using chemical bath deposition (CBD) method without post-heat treatment. *Egypt. J. Chem.* **66**(4), 63–70 (2023)
  63. F. Barreca, N. Acacia, S. Spadaro, G. Curro, F. Neri, Tungsten trioxide (WO<sub>3-x</sub>) nanoparticles prepared by pulsed laser ablation in water. *Mater. Chem. Phys.* **127**, 197 (2011)
  64. M.M. ElFaham, M. Okil, A.M. Mostafa, Effects of post-laser irradiation on the optical and structure properties of Al<sub>2</sub>O<sub>3</sub> nanoparticles produced by laser ablation. *J. Mol. Struct.* **1185**, 351 (2019)
  65. H.D. Abbar, M.A. Fakhri, M.J. AbdulRazzaq, Synthesis gallium nitride on porous silicon nano-structure for optoelectronics devices. *Silicon* **14**(18), 12837–12853 (2022)
  66. O. Yayapao, T. Thongtem, A. Phuruangrat, S. Thongtem, Synthesis and characterization of europium-doped zinc oxide photocatalyst. *J. Alloys Compd* **509**, 2294 (2011)
  67. A. Agrawal, S.H. Cho, O. Zandi, S. Ghosh, R. Johns, D. Milliron, Spectrally tunable infrared plasmonic F, Sn:In<sub>2</sub>O<sub>3</sub> nanocrystal cubes. *Chem. Rev.* **118**, 3121 (2018)
  68. M.A. Fakhri, R.S. Mohammed, Preparation and characterization of titanium dioxide using PLD at various energy of pulsed laser. *Adv. Nat. Sci. Nanosci. Nanotechnol.* **13**(4), 045013 (2022)
  69. R.A. Ismail, A.M. Mousa, M.H. Amin, Effect of laser fluence on the structural, morphological and optical properties of 2H-PbI<sub>2</sub> nanoparticles prepared by laser ablation in ethanol. *J. Inorg. Organomet. Polym Mater.* **28**, 2365–2374 (2018)
  70. N.V. Taranenko, A.V. Butsen, E.A. Nevar, N.A. Savastenko, Synthesis of nanosized particles during laser ablation of gold in water. *Appl. Surf. Sci.* **252**, 4439 (2006)
  71. H.D. Jabbar, M.A. Fakhri, M.J. Abdul Razzaq, O.S. Dahham, E.T. Salim, F.H. Alsultany, Effect of different etching time on fabrication of an optoelectronic device based on GaN/Psi. *J. Renew. Mater.* **11**(3), 1101–1122 (2023)
  72. E.A. Davis, N.F. Mott, Conduction in non-crystalline systems V. Conductivity, optical absorption and photoconductivity in amorphous semiconductors. *Philos. Mag.* **22**(179), 0903–0922 (1970)



73. E.T. Salim, J.A. Saimon, M.K. Abood, F.H. Alsultany, A preliminary study on structural and optical properties of heat treated Nb<sub>2</sub>O<sub>5</sub> nanostructure. *Int. J. Nanoelectron. Mater.* **16**(1), 21–32 (2023)
74. N.K. Hassan, F.G. Khalid, A.A. Ekshayesh, O.S. Dahham, M.M. Hussein, Optical investigations of gold nano rods and gold nano rods doped with ZnO nanoparticles for optoelectronic applications. *J. Opt. (India)* (2023). <https://doi.org/10.1007/s12596-023-01120-1>
75. S. Osamah, A.A. Alwahib, M.A. Fakhri, S.C.B. Gopinath, Study of single and symmetrical D-shaped optical fiber sensor based on gold nanorods. *J. Opt. (India)* (2023). <https://doi.org/10.1007/s12596-023-01119-8>
76. Y.S. Zou, Y.C. Zhang, D. Lou, H.P. Wang, L. Gu, Y.H. Dong, K. Dou, X.F. Song, H.B. Zeng, Structural and optical properties of WO<sub>3</sub> films deposited by pulsed laser deposition. *J. Alloys Compd.* **583**, 465–470 (2014)
77. M.A. Fakhri, A.A. Alwahib, S.F.H. Alhasan, A.W. Abdulwahab, U. Hashim, Optoelectronic device based on lithium niobate nanofilms deposited at various pulsed laser wavelengths. *J. Opt. (India)* (2023). <https://doi.org/10.1007/s12596-023-01173-2>
78. F. Zohreh, D. Dorrani, A.H. Sari, Laser ablation-assisted synthesis of tungsten sub-oxide (W<sub>17</sub>O<sub>47</sub>) nanoparticles in water: effect of laser fluence. *Opt. Quant. Electron.* **52**, 1–16 (2020)
79. R. Bhargava, S. Khan, Fabrication of WO<sub>3</sub>-reduced graphene oxide (WO<sub>3</sub>-G) nanocomposite for enhanced optical and electrical properties. *J. Mater. Sci. Mater. Electron.* **31**, 8370–8384 (2020)
80. E.T. Salim, S.R. Shafeeq, M.J. AbdulRazaq, M.A. Fakhri, S.C.B. Gopinath, Photo-activation of Ag chemicals for enhanced Nb<sub>2</sub>O<sub>5</sub> optoelectronic device employing plasmonic effects. *Surf. Interfaces* **36**, 102618 (2023)
81. K. Lee, W.S. Seo, J.T. Park, Synthesis and optical properties of colloidal tungsten oxide nanorods. *J. Am. Chem. Soc.* **125**, 3408–3409 (2003)
82. M.A. Fakhri, M.J.A. Razaq, H.D. Jabbar, E.T. Salim, F.H. Alsultany, U. Hashim, Fabrication of UV photodetector based on GaN/Psi heterojunction using pulse laser deposition method: effect of different laser wavelengths. *Opt. Mater.* **137**, 113593 (2023)
83. M. Fakhari, M.J. Torkamany, S.N. Mirnia, S.M. Elahi, UV-visible light-induced antibacterial and photocatalytic activity of half harmonic generator WO<sub>3</sub> nanoparticles synthesized by pulsed laser ablation in water. *Opt. Mater.* **85**, 491–499 (2018)
84. M. Moradi, E. Solati, S. Darvishi, D. Dorrani, Effect of aqueous ablation environment on the characteristics of ZnO nanoparticles produced by laser ablation. *J. Cluster Sci.* **27**, 127–138 (2016)
85. E.T. Salim, A.I. Hassan, F.A. Mohamed, M.H.A. Wahid, M.A. Fakhri, A sight of view on electrical impacts, structural properties and surface roughness of tungsten trioxide thin film: effect of substrate temperatures in WO<sub>3</sub>/Si device fabrication. *Phys. Scr.* **98**(3), 035508 (2023)
86. H.A. Jaafar, N.J. Mohammed, Tuning structural and optical properties of WO<sub>3</sub> NPs thin films by the fluency of laser pulses. *Al-Mustansiriyah J. Sci.* **33**(3), 94–100 (2022)
87. M.A. Fakhri, A.A. Alwahib, E.T. Salim, H.A. AbdulAmir, F.H. Alsultany, U. Hashim, Synthesis and characterization of GaN/quartz nanostructure using pulsed laser ablation in liquid. *Phys. Scr.* **97**, 115813 (2022)
88. R.A. Ismail, E.T. Salim, M.S. Alwazny, Nanosecond laser ablation of Au@LiNbO<sub>3</sub> core-shell nanoparticles in ethanol: properties and application in optoelectronic devices. *Plasmonics* **18**(2), 561–576 (2023)
89. B.D. Cullity, *Elements of X-ray diffraction* (Addison-Wesley Publishing, Boston, 1956)
90. M.A. Fakhri, E.T. Salim, S.M. Tariq, R.K. Ibrahim, F.H. Alsultany, A.A. Alwahib, S.F.H. Alhasan, S.C.B. Gopinath, Z.T. Salim, U. Hashim, A gold nanoparticles coated unclad single mode fiber-optic sensor based on localized surface plasmon resonance. *Sci. Rep.* **13**, 5680 (2023)
91. H. Adam, S.C.B. Gopinath, M.K. Md Arshad, S. Sasidharan, Y.S. Wu, Integration of microfluidic channel on electrochemical-based nanobiosensors for monoplex and multiplex analyses: an overview. *J. Taiwan Inst. Chem. Eng.* **146**, 104814 (2023)
92. E.T. Salim, A.T. Hassan, R.O. Mahdi, F.H. Alsultany, Physical properties of HfO<sub>2</sub> nano structures deposited using PLD. *Int. J. Nanoelectron. Mater.* **16**(3), 495–510 (2023)
93. N.J. Mohammed, H.A. Ahmed, Effect of laser fluence on structural transformations and photoluminescence quenching of zinc selenide nanoparticles thin films. *Al-Mustansiriyah J. Sci.* **29**, 122–127 (2018)
94. E.T. Salim, W.K. Khalef, M.A. Fakhri, R.B. Fadhil, A.S. Azzahrani, R.K. Ibrahim, R.A. Ismail, Silver decorated lithium niobate nanostructure by UV activation method for silver–lithium niobate/silicon heterojunction device. *Sci. Rep.* **13**, 11514 (2023)
95. Y. Wang, X. Su, S. Lu, Shape-controlled synthesis of TiO<sub>2</sub> hollow structures and their application in lithium batteries. *J. Mater. Chem.* **22**, 1969 (2012)
96. C. Guo, S. Yin, Q. Dong, T. Sato, The near infrared absorption properties of W<sub>18</sub>O<sub>49</sub>. *RSC Adv.* **2**, 5041–5043 (2012)
97. E.T. Salim, M.A. Fakhri, S.M. Tariq, A.S. Azzahrani, R.K. Ibrahim, A.A. Alwahib, S.F.H. Alhasan, A.T. Ramizy, E.Y. Salih, Z.T. Salim, The unclad single-mode fiber-optic sensor simulation for localized surface plasmon resonance sensing based on silver nanoparticles embedded coating. *Plasmonics* (2023). <https://doi.org/10.1007/s11468-023-01949-z>
98. G.S. Jaber, K.S. Khashan, M.J. Abbas, Study the characteristics optical and structure properties of ZnO-nanoparticles fabricated by laser ablation in liquid. *J. Phys. Conf. Ser.* **1795**, 012004 (2021)
99. E.T. Salim, A.I. Hassan, F.A. Mohamed, M.A. Fakhri, A.J. Addie, Optical and electrical investigations of tungsten trioxide for optoelectronics devices. *J Mater Sci. Mater Electron.* **34**, 1546 (2023)
100. W.T. Nichols, T. Sasaki, N. Koshizaki, Laser ablation of a platinum target in water. III. Laser-induced reactions. *J. Appl. Phys.* **100**, 114911 (2006)
101. R. Intartaglia, K. Bagga, M. Scotto, A. Diaspro, F. Brandi, Luminescent silicon nanoparticles prepared by ultra short pulsed laser ablation in liquid for imaging applications. *Opt. Mater. Express* **2**, 510–518 (2012)
102. M.A. Fakhri, E.T. Salim, G.M. Sulaiman, S. Albukhaty, H.S. Ali, Z.T. Salim, S.C.B. Gopinath, U. Hashim, Z.T. Al-aqbi, Gold nanowires based on photonic crystal fiber by laser ablation in liquid to improve colon biosensor. *Plasmonics* (2023). <https://doi.org/10.1007/s11468-023-01961-3>
103. H. Imam, K. Elsayed, M.A. Ahmed, R. Ramdan, Effect of experimental parameters on the fabrication of gold nanoparticles via laser ablation. *Opt. Photonics J.* **2**(2), 73–84 (2012)
104. V. Piriya Wong, V. Thongpool, P. Asanithi, P. Limsuwan, Preparation and characterization of alumina nanoparticles in deionized water using laser ablation technique. *J. Nanomater.* (2012). <https://doi.org/10.1155/2012/819403>
105. M.A. Fakhri, A.A. Alwahib, E.T. Salim, R.A. Ismail, H.A.A.A. Amir, R.K. Ibrahim, S.F.H. Alhasan, F.H. Alsultany, Z.T. Salim, S.C.B. Gopinath, Preparation and characterization of UV-enhanced GaN/porous Si photodetector using PLA in liquid. *Silicon* (2023). <https://doi.org/10.1007/s12633-023-02528-x>

**Publisher's Note** Springer Nature remains neutral with regard to jurisdictional claims in published maps and institutional affiliations.

Springer Nature or its licensor (e.g. a society or other partner) holds exclusive rights to this article under a publishing agreement with the author(s) or other rightsholder(s); author self-archiving of the accepted

manuscript version of this article is solely governed by the terms of such publishing agreement and applicable law.